**Proceedings of the ASME 2017 Dynamic Systems and Control Conference**
**DSCC 2017**
**October 11-13, 2017, Tysons Corner, Virginia, USA**

**DSCC2017-5006**

# SUPPRESSING CHAOTIC/HYPERCHAOTIC DYNAMICS OF SMART VALVES NETWORK USING DECENTRALIZED AND CENTRALIZED SCHEMES

**Peiman Naseradinmousavi and Mostafa Bagheri**
Dynamic Systems and Control Laboratory
Department of Mechanical Engineering
San Diego State University, San Diego, USA

**Hashem Ashrafiuon**
Director of Center for Nonlinear Dynamics and Control
Department of Mechanical Engineering
Villanova University, Villanova, USA

**Marcello Canova**
Department of Mechanical & Aerospace Engineering
Ohio State University, Columbus, USA

**David B. Segala**
Naval Undersea Warfare Center
1176 Howell Street, Newport, USA

## ABSTRACT

*In this effort, we present a comprehensive comparative study of decentralized and centralized adaptive schemes to control the so-called "Smart Valves" network employed in many applications including, but not limited to, Municipal Piping Systems and oil and gas fields. The network being considered here typically includes scores of coupled solenoid actuated butterfly valves. We here examine the multiphysics network of two interconnected actuated sets. The network undergoes the coupled chaotic and hyperchaotic dynamics subject to some initial conditions and critical parameters. The control schemes' trade-offs are thoroughly investigated with respect to robustness, computational cost, and practical feasibility of control inputs in the presence of strong nonlinear interconnections and harmful chaotic and hyperchaotic responses.*

## 1 Introduction

The decentralized and centralized control of large-scale networks have received considerable attention, particularly in the presence of coupled harmful responses. The coupled dangerous dynamical responses, including chaotic and hyperchaotic (with larger domain of attraction) ones, can be transmitted among neighbor sets. Consequently, robust and practically feasible control schemes are needed to be implemented in driving such large-scale systems.

The system being studied here is the so-called "Smart Valves" network containing scores of interconnected actuated butterfly valves coupled in series. This multiphysics system broadly deals with several aspects of electro-magneto-mechanical-fluid units. We particularly analyze two sets of coupled bi-directional solenoid actuated butterfly valves. The network plays an important role in proper and efficient performance of many critical infrastructures which include, but are not limited to, the US Navy, oil and gas fields, petrochemical plants, and more importantly, **M**unicipal **P**iping **S**ystems. The first utilizes a distributed flow control system for cooling purposes and therefore, the failure of such a crucial unit would expectedly impose considerable costs of restoration and operation. A robust and practically feasible control scheme is hence required to mitigate the effects of the harmful dynamic responses in the presence of uncertainties involved with such a large-scale network.

We have previously reported broad analytical and experimental studies [1–13] for both an isolated actuator-valve arrangement and a network of two interconnected solenoid actuated butterfly valves operating in series. Novel third-order (nondimensional) and sixth-order analytical models of the single and two sets of solenoid actuated butterfly valves were derived, respectively, dealing with the coupled nonlinear magnetic, hydrodynamic, and bearing torques. The transient chaotic and crisis,

and coupled chaotic and hyperchaotic dynamics of both the single and interconnected sets were captured, respectively, by exposing the system to some critical parameters and initial conditions. The constrained isolated and then coupled design and operational optimization problems were solved using the stability constraints imposed by the dynamic analysis. Finding specific research work to capture and control the chaotic and hyperchaotic dynamics of such a multiphysics network, using both the centralized/decentralized schemes, is somewhat difficult although some efforts have been reported for similar case studies. Many efforts have been addressed in [14–28] to thoroughly investigate the decentralized and centralized schemes for a variety of electromechanical systems.

We here briefly represent the interconnected analytical model of two sets (for completeness) along with the critical initial conditions and parameters resulted in the dangerous responses. Both the centralized (coupled) and decentralized adaptation and control laws will be formulated with respect to the interconnected dynamics of the system; in the presence of chaotic and hyperchaotic responses. The results will be thoroughly discussed to address the practical feasibility and robustness of both the adaptive methods, for vanishing the chaotic and hyperchaotic dynamics, in addition to their computational costs.

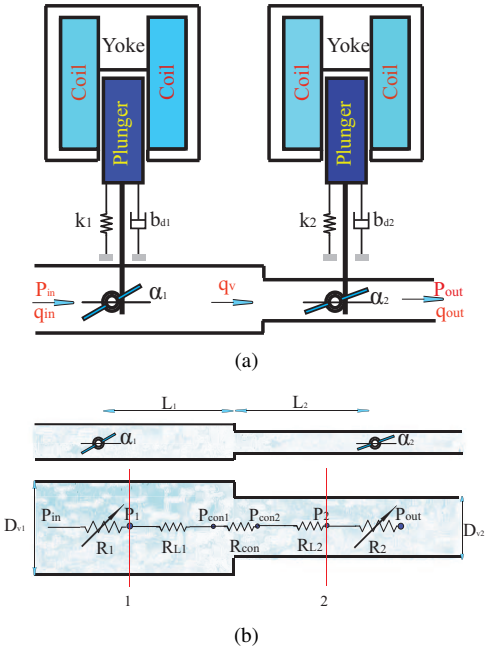


**FIGURE 1**. (a) A schematic configuration of two bi-directional solenoid actuated butterfly valves subject to the sudden contraction; (b) A coupled model of two butterfly valves in series without actuation

## 2 Mathematical Modeling

The system, which is being considered here, is two bi-directional solenoid actuated butterfly valves operating in series. The system undergoes a sudden pipe contraction as shown in Fig 1. The plungers are connected to the valves' stems through the rack and pinion arrangements yielding kinematic constraints.

We have previously derived the interconnected analytical model of two sets operating in series [1–4] and briefly represent here for completeness. Some simplifying assumptions have been made to develop the analytical formulas of the coupled sets. The first one is to assume a negligible magnetic "diffusion time" with respect to a nominal operation time (40s). Note that the diffusion time has an inverse relationship with the amount of current applied. The second assumption is the existence of laminar flow. We have carried out experimental work for an isolated set to validate the assumption of laminar flow. The total flow loads, including hydrodynamic ($T_h$) and bearing ($T_b$) torques, were measured experimentally. An acceptable consistency was observed between the analytical and experimental approaches [29].

Based on the analytical formulas addressed in [1–4], the sixth-order interconnected dynamic equations of two bi-directional solenoid actuated butterfly valves were developed as follows:

$$\dot{z}_1 = z_2 \tag{1}$$

$$\dot{z}_2 = \frac{1}{J_1}\left[\frac{r_1 C_{21} N_1^2 z_3^2}{2(C_{11}+C_{21}(g_{m1}-r_1 z_1))^2} - b_{d1} z_2 - k_1 z_1 + \frac{\frac{(P_{in}-P_{out}-(R_{L1}+R_{L2}+R_{con}q_v)q_v)e_1}{(p_1 z_1^3+q_1 z_1^2+o_1 z_1+\gamma_1)^2}}{\sum_{i=1,4}\frac{e_i}{(p_i z_i^3+q_i z_i^2+o_i z_i+\gamma_i)^2}} \times \left[(a_1 z_1 e^{b_1 z_1{}^{1.1}} - c_1 e^{d_1 z_1}) - C_1 \times \tanh(K z_2)\right]\right] \tag{2}$$

$$\dot{z}_3 = \frac{(V_1 - R_1 z_3)(C_{11}+C_{21}(g_{m1}-r_1 z_1))}{N_1^2} - \frac{r_1 C_{21} z_3 z_2}{(C_{11}+C_{21}(g_{m1}-r_1 z_1))} \tag{3}$$

$$\dot{z}_4 = z_5 \tag{4}$$

$$\dot{z}_5 = \frac{1}{J_2}\left[\frac{r_2 C_{22} N_2^2 z_6^2}{2(C_{12}+C_{22}(g_{m2}-r_2 z_4))^2} - b_{d2} z_5 - k_2 z_4 + \frac{\frac{(P_{in}-P_{out}-(R_{L1}+R_{L2}+R_{con}q_v)q_v)e_2}{(p_2 z_4^3+q_2 z_4^2+o_2 z_4+\gamma_2)^2}}{\sum_{i=1,4}\frac{e_i}{(p_i z_i^3+q_i z_i^2+o_i z_i+\gamma_i)^2}} \times \left[(a_1' z_4 e^{b_1' z_4{}^{1.1}} - c_1' e^{d_1' z_4}) - C_2 \times \tanh(K z_5)\right]\right] \tag{5}$$

$$\dot{z}_6 = \frac{(V_2 - R_2 z_6)(C_{12}+C_{22}(g_{m2}-r_2 z_4))}{N_2^2} - \frac{r_2 C_{22} z_5 z_6}{(C_{12}+C_{22}(g_{m2}-r_2 z_4))} \tag{6}$$

where, $b_{di}$ indicates the equivalent torsional damping, $k_i$ is the

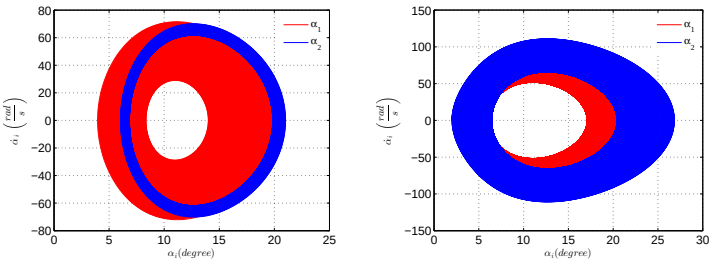


(a) (b)

**FIGURE 2**. (a) The coupled sets' phase portraits for Initial$_1$; (b) The coupled sets' phase portraits for Initial$_2$

equivalent torsional stiffness, $V_i$ stands for the supply voltage, $r_i$ indicates the radius of the pinion, $C_1$ and $C_2$ are the reluctances of the magnetic path without air gap and that of the air gap, respectively, $N_i$ stands for the number of coils, $g_{mi}$ is the nominal air gap, $J_i$ indicates the polar moment of inertia of the valve's disk, and $R_i$ is the electrical resistance of coil. $z_1 = \alpha_1$, $z_2 = \dot{\alpha}_1$, and $z_3 = i_1$ indicate the upstream valve's rotation angle, angular velocity, and actuator current, respectively. $z_4 = \alpha_2$, $z_5 = \dot{\alpha}_2$, and $z_6 = i_2$ stand for the downstream valve's rotation angle, angular velocity, and actuator current, respectively. The network parameters are listed in Table 1.

Note that we could capture, for the first time, the coupled chaotic and hyperchaotic dynamics of the interconnected sets [1, 3] by examining the critical values of $b_{di} = \mu_i = 1 \times 10^{-7}$ for two different initial conditions of Initial$_1$ = $[20(deg)\ 0\ 0\ 20(deg)\ 0\ 0]$ and Initial$_2$ = $[2(deg)\ 0\ 0\ 2(deg)\ 0\ 0]$, respectively. Shown in Figs. 2(a) and 2(b) are the chaotic and hyperchaotic dynamics of the coupled actuated valves, respectively. Some powerful tools of the nonlinear analysis, including the Lyapunov exponents and Poincaré map [30], were used in distinguishing among the nature of harmful responses, as shown in Figs. 3(a)-3(f). One and two positive Lyapunov exponents along with irregular Poincaré maps confirmed the chaotic and hyperchaotic dynamics of the actuated valves, respectively. Such dangerous responses need to be vanished using a nonlinear control scheme, due to the nonlinear and coupled nature of the network, in order to return the interconnected sets to their stable domains. The operationally optimized valves' motions, on the other hand, are utilized in the nonlinear control scheme as desirable trajectories. Based on the inevitable unknown parameters of such a coupled network, the nonlinear model-based adaptive scheme looks as an effective approach to be employed in stabilizing the system subject to the chaotic and hyperchaotic dynamics.

**TABLE 1**. The system parameters

| | | | |
|---|---|---|---|
| $\rho$ | $1000\frac{kg}{m^3}$ | $v$ | $3\frac{m}{s}$ |
| $J_{1,2}$ | $0.104 \times 10^{-1}(kg.m^2)$ | $N_2$ | 3300 |
| $N_1$ | 3300 | $C_{11,22}$ | $1.56 \times 10^6(H^{-1})$ |
| $D_{v1}$ | 0.2032(m) | $D_{v2}$ | 0.127(m) |
| $D_{s1,s2}$ | 0.01(m) | $P_{out}$ | 2(kPa) |
| $k_{1,2}$ | $60(N.m^{-1})$ | $C_{21,22}$ | $6.32 \times 10^8(H^{-1})$ |
| $L_1$ | 2(m) | $L_2$ | 1(m) |
| $r_{1,2}$ | 0.05(m) | $\theta$ | 90° |
| $P_{in}$ | 256(kPa) | $g_{m1,m2}$ | 0.1(m) |
| $\mu_f$ | 0.018 $(Kg.m^{-1}.s^{-1})$ | $\lambda_{1,2}$ | 1 |
| $n_{1,2}$ | 10 | $b_{di} = \mu_i$ | $1 \times 10^{-7}$ |
| $\varepsilon_{1,2}$ | $5 \times 10^{-3}$ | $e_1$ | $7.2 \times 10^5$ |
| $p_1$ | 461.9 | $q_1$ | -405.4 |
| $o_1$ | -1831 | $\gamma_1$ | 2207 |
| $e_2$ | $4.51 \times 10^5$ | $p_2$ | 161.84 |
| $q_2$ | -110.53 | $o_2$ | -695.1 |
| $\gamma_2$ | 807.57 | | |

## 3 Control and Adaptation Laws

### 3.1 Adaptive Centralized Approach

The nonlinear model-based adaptive control method [31] is used in stabilizing the unstable system in order to track the desired trajectories [1, 3] defined based on the critical initial conditions as follows:

$$\alpha_{di} = \frac{\pi}{3}\tanh(10^{-4}t^3) + \frac{\pi}{9},\ \text{Initial}_1 \tag{7}$$

$$\alpha_{di} = \frac{\pi}{3}\tanh(10^{-4}t^3) + \frac{\pi}{90},\ \text{Initial}_2 \tag{8}$$

The so-called "S-Shaped" trajectories are highly energy-efficient [3, 9] and yield smooth dynamic responses avoiding the repeatedly observed dangerous phenomenon of "Water Hammering". The coupled dynamic Eqs. 2 and 5 can be rewritten as the following:

$$J_i\ddot{\alpha}_i + b_{di}\dot{\alpha}_i + k_i\alpha_i = \frac{r_i C_{2i} N_i^2 i_i^2}{2(C_{1i} + C_{2i}(g_{mi} - r_i\alpha_i))^2}$$

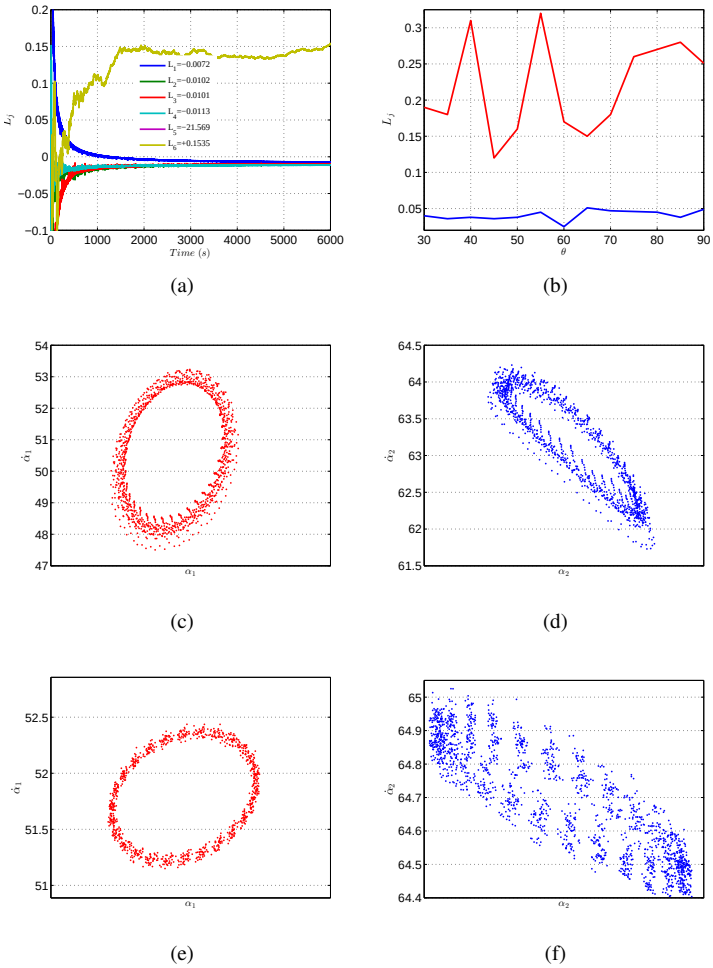


**FIGURE 3**. (a) The Lyapunov exponents for Initial$_1$; (b) The positive Lyapunov exponents for Initial$_2$ vs. different approach angles ($\theta$); (c) The poincaré map for Initial$_1$ of the upstream set; (d) The poincaré map for Initial$_1$ of the downstream set; (e) The Poincaré map for Initial$_2$ of the upstream set; (f) The poincaré map for Initial$_2$ of the downstream set

$$+\frac{A_1 R_{ni}}{\sum_{i=1}^{2} R_{ni}}[T'_{hi} - T'_{bi}\tanh(K\dot{\alpha}_i)],\ (i=1,2) \tag{9}$$

where, $A_1 = (P_{in} - P_{out} - (R_{L1} + R_{L2} + R_{con}q_v)q_v)$, $T'_{h1} = a_1\alpha_1 e^{b_1{\alpha_1}^{1.1}} - c_1 e^{d_1\alpha_1}$, $T'_{h2} = a'_1\alpha_2 e^{b'_1{\alpha_2}^{1.1}} - c'_1 e^{d'_1\alpha_2}$, and $T'_{bi} = 0.5A_{di}\mu_i D_{si}$. Assuming,

$$M_i = \frac{2J_i(C_{1i}+C_{2i}(g_{mi}-r_i\alpha_i))^2}{r_i C_{2i} N_i^2}, B_i = \frac{2b_{di}(C_{1i}+C_{2i}(g_{mi}-r_i\alpha_i))^2}{r_i C_{2i} N_i^2}$$

$$K_i = \frac{2k_i(C_{1i}+C_{2i}(g_{mi}-r_i\alpha_i))^2}{r_i C_{2i} N_i^2}, Co_i = \frac{2(C_{1i}+C_{2i}(g_{mi}-r_i\alpha_i))^2}{r_i C_{2i} N_i^2}$$

Eq. 9 can be rewritten as follows.

$$M_i\ddot{\alpha}_i + B_i\dot{\alpha}_i + K_i\alpha_i = u_i + \frac{A_1 Co_i R_{ni}}{\sum_{i=1}^{2} R_{ni}}[T'_{hi} - T'_{bi}\tanh(K\dot{\alpha}_i)],\ (i=1,2) \tag{10}$$

We define the valves' tracking errors and their first and second time derivatives as the following:

$$e_i = \alpha_{di} - \alpha_i, \dot{e}_i = \dot{\alpha}_{di} - \dot{\alpha}_i, \ddot{e}_i = \ddot{\alpha}_{di} - \ddot{\alpha}_i,\ (i=1,2)$$

This yields,

$$M_i\ddot{e}_i = M_i\ddot{\alpha}_{di} - M_i\ddot{\alpha}_i = M_i\ddot{\alpha}_{di} + B_i\dot{\alpha}_i + K_i\alpha_i - u_i - \frac{A_1 Co_i R_{ni}}{\sum_{i=1}^{2} R_{ni}}[T'_{hi} - T'_{bi}\tanh(K\dot{\alpha}_i)],\ (i=1,2) \tag{11}$$

The combined tracking errors [31] and their first time derivatives are as follows:

$$s_i = \dot{e}_i + \lambda_i e_i, \dot{s}_i = \ddot{e}_i + \lambda_i\dot{e}_i,\ (i=1,2)$$

where $\lambda$'s are strictly positive numbers listed in Table 1. Premultiplying by $M_i$ and substituting from Eq. 11, we have,

$$M_i\dot{s}_i = M_i\ddot{\alpha}_{di} + B_i\dot{\alpha}_i + K_i\alpha_i - u_i + M_i\lambda_i\dot{e}_i - \frac{A_1 Co_i R_{ni}}{\sum_{i=1}^{2} R_{ni}}[T'_{hi} - T'_{bi}\tanh(K\dot{\alpha}_i)],\ (i=1,2) \tag{12}$$

Based on the interconnected dynamics of the network, we chose the following quadratic Lyapunov function candidate:

$$V = \frac{1}{2}\left[\sum_{i=1}^{2}(s_i^T M_i s_i + \tilde{\Theta}_i^T\Gamma_i^{-1}\tilde{\Theta}_i)\right] \tag{13}$$

where $\Gamma_i$ is a symmetric positive definite matrix and $\tilde{\Theta}_i$ is the system's lumped parameter estimation error ($\tilde{\Theta}_i = \Theta_i - \hat{\Theta}_i$). Differentiating the Lyapunov function (Eq. 13) yields,

$$\dot{V} = \sum_{i=1}^{2}(s_i^T M_i\dot{s}_i + \frac{1}{2}s_i^T\dot{M}_i s_i - \tilde{\Theta}_i^T\Gamma_i^{-1}\dot{\hat{\Theta}}_i) \tag{14}$$

By defining the regression vectors as the following:

$$W_i\Theta_i = M_i\ddot{\alpha}_{di} + B_i\dot{\alpha}_i + K_i\alpha_i - \frac{A_1 Co_i R_{ni}}{\sum R_{ni}} \times [T'_{hi} - T'_{bi}\tanh(K\dot{\alpha}_i)] + M_i\lambda_i\dot{e}_i + \frac{1}{2}\dot{M}_i s_i,\ (i=1,2) \quad (15)$$

The $\dot{V}$ can be easily rewritten as follows.

$$\dot{V} = \sum_{i=1}^{2}\left[s_i^T[W_i\Theta_i - u_i] - \tilde{\Theta}_i^T\Gamma_i^{-1}\dot{\hat{\Theta}}_i\right] \quad (16)$$

The appropriate control inputs are hence chosen as the following:

$$u_i = W_i\hat{\Theta}_i + n_i s_i,\ (i=1,2) \quad (17)$$

where,

$$W_i\hat{\Theta}_i = \hat{M}_i\ddot{\alpha}_{di} + \hat{B}_i\dot{\alpha}_i + \hat{K}_i\alpha_i - \frac{A_1\hat{C}o_i R_{ni}}{\sum R_{ni}} \times [T'_{hi} - T'_{bi}\tanh(K\dot{\alpha}_i)] + \hat{M}_i\lambda_i\dot{e}_i + \frac{1}{2}\hat{\dot{M}}_i s_i,\ (i=1,2) \quad (18)$$

We can easily develop the regression ($W_i \in \Re^{1\times 17}$) (and subsequently estimated lumped parameter vectors ($\hat{\Theta}_i \in \Re^{17\times 1}$)) as follows.

$$W_i = \big[\alpha_i^2\ddot{\alpha}_{di}, \alpha_i\ddot{\alpha}_{di}, \ddot{\alpha}_{di}, \alpha_i^2\dot{\alpha}_i, \alpha_i\dot{\alpha}_i, \dot{\alpha}_i, \alpha_i^3, \alpha_i^2, \alpha_i, \frac{A_1R_{ni}}{\sum R_{ni}}[T'_{hi} - T'_{bi}\tanh(K\dot{\alpha}_i)]\alpha_i^2, \frac{A_1R_{ni}}{\sum R_{ni}}[T'_{hi} - T'_{bi}\tanh(K\dot{\alpha}_i)]\alpha_i, \frac{A_1R_{ni}}{\sum R_{ni}}[T'_{hi} - T'_{bi}\tanh(K\dot{\alpha}_i)], \alpha_i^2\dot{e}_i, \alpha_i\dot{e}_i, \dot{e}_i, \alpha_i s_i, s_i\big], (i=1,2) \quad (19)$$

Substituting the control inputs into Eq. 16 gives,

$$\dot{V} = \sum_{i=1}^{2} s_i^T[\underbrace{W_i\Theta_i - W_i\hat{\Theta}_i}_{W_i\tilde{\Theta}_i} - n_i s_i] - \tilde{\Theta}_i^T\Gamma_i^{-1}\dot{\hat{\Theta}}_i$$
$$= \sum_{i=1}^{2} s_i^T W_i\tilde{\Theta}_i - s_i^T n_i s_i - \tilde{\Theta}_i^T\Gamma_i^{-1}\dot{\hat{\Theta}}_i$$
$$= \sum_{i=1}^{2}[s_i^T W_i - \Gamma_i^{-1}\dot{\hat{\Theta}}_i^T]\tilde{\Theta}_i - s_i^T n_i s_i \quad (20)$$

which leads us to develop the following parameters' adaptation laws:

$$\dot{\hat{\Theta}}_i = \Gamma_i W_i^T s_i \quad (21)$$

Substituting Eq. 21 into Eq. 20 yields,

$$\dot{V} = \sum_{i=1}^{2} -s_i^T n_i s_i \le 0 \quad (22)$$

Based on Eq. 22, we need to prove $\dot{V}\to 0$ as $t\to\infty$ revealing $s_i\to 0$ when $t\to\infty$, or simply:

$$\dot{V}\to 0 \Rightarrow s_i\to 0$$

Since $V$ is positive, Barbalat's lemma [31] confirms that $\dot{V}$ approaches zero if it is uniformly continuous and its time derivative $\ddot{V}$ is bounded:

$$\ddot{V} \text{ is bounded} \Rightarrow \dot{V}\to 0 \Rightarrow s_i\to 0$$

We can easily derive $\ddot{V}$ as follows.

$$\ddot{V} = -2\sum_{i=1}^{2} s_i^T n_i\dot{s}_i \quad (23)$$

Eq. 23 implies,

$$s_i \text{ and } \dot{s}_i \text{ are bounded} \Rightarrow \ddot{V} \text{ is bounded} \Rightarrow \dot{V}\to 0 \Rightarrow s_i\to 0$$

Note that $V$ is bounded due to $V\ge 0$ and $\dot{V}\le 0$ indicating that $s_i$ and $\tilde{\Theta}_i$ are also bounded. This would in turn reveals that $\alpha_i$, $\dot{\alpha}_i$, $\alpha_{di}$, $\dot{\alpha}_{di}$, $\ddot{\alpha}_{di}$ ($s_i = f(\alpha_i, \dot{\alpha}_i, \dot{\alpha}_{di}, \alpha_{di})$), and $\hat{\Theta}_i$ are bounded. Combining Eqs. 12, 15, and 17 gives,

$$M_i\dot{s}_i + \left[n_i + \frac{1}{2}\dot{M}_i\right]s_i = W_i\tilde{\Theta}_i,\ (i=1,2) \quad (24)$$

Note that the bounded $\alpha_i$ and $\dot{\alpha}_i$ result in bounded $M_i$ and $\dot{M}_i$ yielding bounded $\dot{s}_i$ due to the bounded $s_i$, $W_i$, and $\tilde{\Theta}_i$. The bounded $s_i$ and $\dot{s}_i$ result in the bounded $\dot{V}$ and one can easily conclude that $\dot{V}$ and $s_i\to 0$ as $t\to\infty$ [31]. This obviously indicates that $e_i$ and $\dot{e}_i$ tend to zero as $t\to\infty$. We hence can guarantee both the global stability of the coupled network (the boundedness of

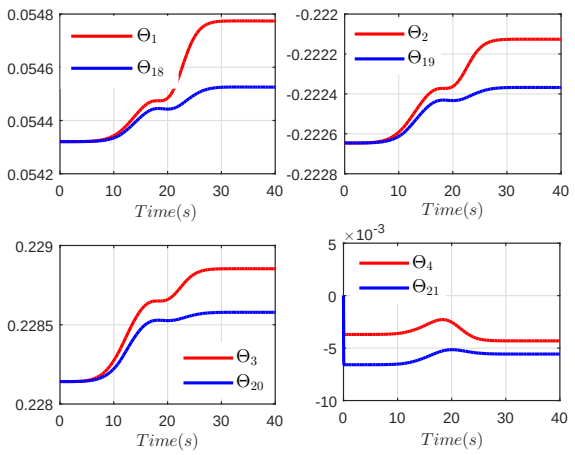


(a)

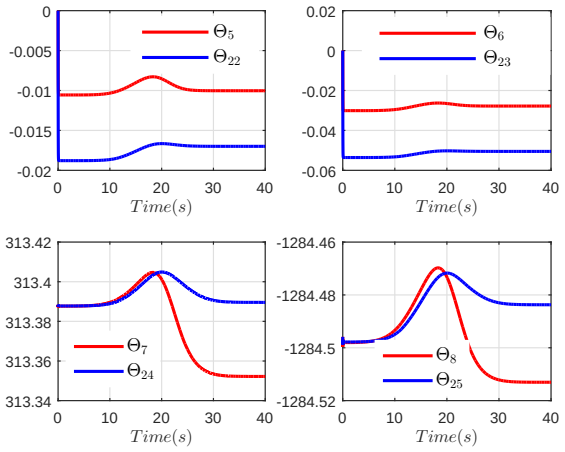


(b)

**FIGURE 4**. The centralized scheme's parameter estimation for $\Theta_1$ to $\Theta_8$ of the upstream set and $\Theta_{18}$ to $\Theta_{25}$ of the downstream set.

$\alpha_i$, $\dot{\alpha}_i$, and $\hat{\Theta}_i$) and convergence of the tracking errors ($e_i$).

### 3.2 Adaptive Decentralized Approach

The decentralized scheme addressed in [32, 33] is used in suppressing the chaotic/hyperchaotic dynamics of the two strongly interconnected sets. We represent the formulations, the direct decentralized adaptation and control laws, for completeness although the detailed stability proof can be easily found in [34]. A large-scale network containing $N$ interconnected sets, here $N = 2$ (Eq. 10), can be generally written in the form of:

$$\dot{\mathbf{x}}_i = F_i(\mathbf{x}_1, ..., \mathbf{x}_N) + g_i(\mathbf{x}_i)u_i \quad (25)$$

$$y_i = h_i(\mathbf{x}_1, ..., \mathbf{x}_N) \quad (26)$$

where, $\mathbf{x}_i = [x_{i,1}, x_{i,2}, ..., x_{i,m_i}]^T$ is the state vector of $i$th set, $\mathbf{x} = [\mathbf{x}_1^T, \mathbf{x}_2^T, ..., \mathbf{x}_N^T]^T$ indicates the full state of the whole network, and $F_i(.)$, $g_i(.)$, and $h(.)$ are smooth functions. $u_i$ and $y_i$ stand for the decentralized input and output of the $i$th set, respectively. The output dynamics of the $i$th set, by having strong relative degree of $n_i$, can be written as follows.

$$y_i^{(n_i)} = \sum_{w=1}^{l} \zeta_{i,w} f_{i,w}(\mathbf{x}_i) + \eta_i u_i + \Delta_i(\mathbf{x}_1, ..., \mathbf{x}_N), (i = 1, 2) \quad (27)$$

where, $y_i^{(n_i)}$ indicates the $n_i$th time derivative of $y_i$, and $\zeta_{i,w}$ and $\eta_i$ are unknown parameters which will be decentrally estimated. Note that there is no assumption on sign of $\eta_i$ ($\eta_i \neq 0$) and $\Delta_i(\mathbf{x}_1, ..., \mathbf{x}_N) \leq \varepsilon_i$ ($\varepsilon_i > 0$) stands for the effects of the other interconnected sets. As defined for the centralized scheme, the tracking error signal is $e_i = \underbrace{r_{di}}_{\alpha_{di}} - \underbrace{y_i}_{\alpha_i}, (i = 1, 2)$. The aim is to design a decentralized adaptive scheme for each set such that the outputs $y_i (i = 1, 2)$ track the desirable trajectories (Eqs. 7 & 8) with respect to the existing strong nonlinear interconnections among the two sets by using only local measurements.

The error vector of the $i$th set is written as $\mathbf{e}_i = [e_i, \dot{e}_i, ..., e_i^{(n_i-1)}]^T$ leading to the following time derivative:

$$\dot{\mathbf{e}}_i = [\dot{e}_i, e_i^{(2)}, ..., e_i^{(n_i)}]^T, (i = 1, 2) \quad (28)$$

We can easily write the error dynamics as follows:

$$e_i^{(n_i)} = r_{di}^{(n_i)} - y_i^{(n_i)}, (i = 1, 2) \quad (29)$$

Substituting Eq. 27 into Eq. 29 yields,

$$e_i^{(n_i)} = r_{di}^{(n_i)} - \sum_{w=1}^{5} \zeta_{i,w} f_{i,w}(\mathbf{x}_i) - \eta_i u_i - \Delta_i, (i = 1, 2) \quad (30)$$

where, $f_{i,1} = \tanh(K\dot{\alpha}_i), f_{1,2} = \alpha_1 e^{b_1 \alpha_1^{1.1}}, f_{i,3} = \alpha_i, f_{i,4} = \dot{\alpha}_i, f_{1,5} = e^{d_1 \alpha_1}, f_{2,2} = \alpha_2 e^{b_1' \alpha_2^{1.1}}, f_{2,5} = e^{d_1' \alpha_2}$, and the corresponding $\zeta_{i,w}$ and $\eta_i$ are estimated through adaptation laws; $\zeta_{i,1} = 0.5 A_{di} \mu_i D_{si}, \zeta_{1,2} = a_1, \zeta_{i,3} = k_i, \zeta_{i,4} = b_{di}, \zeta_{1,5} = c_1, \zeta_{2,2} = a_1', \zeta_{2,5} = c_1'$.

The tracking error of the $i$th set needs to follow $e_i^{(n_i)} + a_{i,n_i-1} e_i^{(n_i-1)} + ... + a_{i,0} e_i = 0$ such that $L_i(s) = s^{(n_i)} + a_{i,n_i-1} s^{(n_i-1)} + ... + a_{i,0}$ is Hurwitz. The decentralized control

signal of the $i$th set is calculated as follows:

$$u_i = \frac{\nu_i}{\hat{\eta}_i} \tag{31}$$

where,

$$\begin{aligned}\nu_i = &\left(a_{i,0}e_i + a_{i,1}\dot{e}_i + a_{i,2}e_i^{(2)} + \ldots + a_{i,n_i-1}e_i^{(n_i-1)}\right) \\ &- \sum_{w=1}^{5} \hat{\zeta}_{i,w} f_{i,w}(\mathbf{x}_i) + r_{di}^{(n_i)} \\ &+ \varepsilon_i \text{sign}(\mathbf{e}_i^T P_i \mathbf{b}_i^T), i = (1,2)\end{aligned} \tag{32}$$

Substituting Eq. 31 into Eq. 30, with respect to $\frac{\eta_i}{\hat{\eta}_i} = 1 - \frac{\tilde{\eta}_i}{\hat{\eta}_i}$

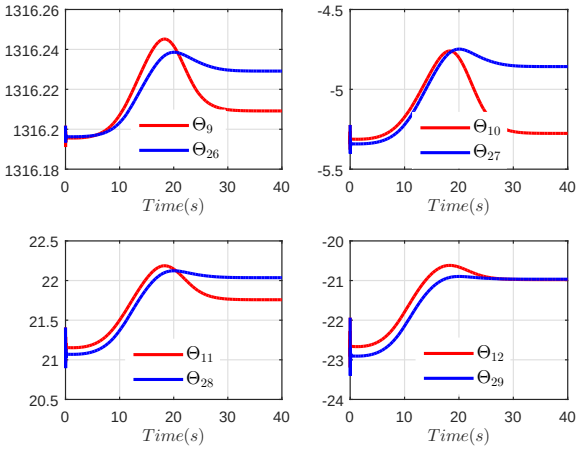


**FIGURE 5**. The centralized scheme's parameter estimation for $\Theta_9$ to $\Theta_{12}$ of the upstream set and $\Theta_{26}$ to $\Theta_{29}$ of the downstream set.

where $\tilde{\eta}_i = \hat{\eta}_i - \eta_i$, the error dynamics becomes,

$$e_i^{(n_i)} = r_{di}^{(n_i)} - \sum_{w=1}^{5} \zeta_{i,w} f_{i,w}(\mathbf{x}_i) - \nu_i + \frac{\tilde{\eta}_i}{\hat{\eta}_i}\nu_i - \Delta_i, (i = 1,2) \tag{33}$$

Combining Eqs. 32 and 33 yields,

$$\begin{aligned}e_i^{(n_i)} = &\sum_{w=1}^{5} \tilde{\zeta}_{i,w} f_{i,w}(\mathbf{x}_i) - \varepsilon_i \text{sign}(\mathbf{e}_i^T P_i \mathbf{b}_i^T) \\ &- \left(a_{i,0}e_i + a_{i,1}\dot{e}_i + a_{i,2}e_i^{(2)} + \ldots + a_{i,n_i-1}e_i^{(n_i-1)}\right) \\ &+ \frac{\tilde{\eta}_i}{\hat{\eta}_i}\nu_i - \Delta_i, (i = 1,2)\end{aligned} \tag{34}$$

where $\tilde{\zeta}_{i,w} = \hat{\zeta}_{i,w} - \zeta_{i,w}$. The error dynamics of the $i$th set, by substituting Eq. 34 into Eq. 28, can be developed as the following matrix form:

$$\begin{aligned}\dot{\mathbf{e}}_i = &A_i\mathbf{e}_i + \mathbf{b}_i \left( \sum_{w=1}^{5} \tilde{\zeta}_{i,w} f_{i,w}(\mathbf{x}_i) - \varepsilon_i \text{sign}(\mathbf{e}_i^T P_i \mathbf{b}_i^T) + \frac{\tilde{\eta}_i}{\hat{\eta}_i}\nu_i \right. \\ &\left. - \Delta_i \right), (i = 1,2)\end{aligned} \tag{35}$$

The Hurwitz matrix $A_i$ and vector $\mathbf{b}_i$ for the two interconnected sets subject to the chaotic and hyperchaotic dynamics are chosen as follows.

$$\begin{aligned}A_i &= \begin{bmatrix} 0 & 1 \\ -\underbrace{1}_{a_{i,0}} & -\underbrace{7\times 10^7}_{a_{i,1}} \end{bmatrix} \\ \mathbf{b}_i &= [0\ 1]^T\end{aligned} \tag{36}$$

The Hurwitz $A_i$ leads to a unique positive definite $P_i$ to be obtained through the Lyapunov equation:

$$A_i^T P_i + P_i A_i = -Q_i \tag{37}$$

where $Q_i$ is a positive definite matrix in which we select as follows (for the two coupled sets):

$$Q_i = \begin{bmatrix} \mathrm{q}_i & 0 \\ 0 & \mathrm{q}_i \end{bmatrix} \times 10^3 \tag{38}$$

where $q_i$=0.1 and $q_i$=0.8 for the chaotic and hyperchaotic responses, respectively. The following decentralized adaptation laws [32, 33] are used in estimating the unknown parameters:

$$\dot{\hat{\zeta}}_{i,w} = -\gamma_{\zeta i} f_{i,w} \mathbf{e}_i^T P_i \mathbf{b}_i^T \tag{39}$$

$$\dot{\hat{\eta}}_i = -\gamma_{\eta i} \frac{\mathbf{e}_i^T P_i \mathbf{b}_i^T \nu_i}{\hat{\eta}_i}, (i = 1,2) \tag{40}$$

where $\gamma_{\zeta i} = \gamma_{\eta i} = 0.1$. The decentralized control and adaptation laws developed through Eqs. 31, 39, and 40 guarantee [34] asymptotic convergence of the tracking errors to zero and also boundedness of the closed-loop network. We have implemented the decentralized formulations in MATLAB to be compared with the centralized scheme with respect to the computational cost,

feasibility, and robustness issues.

## 4 Results

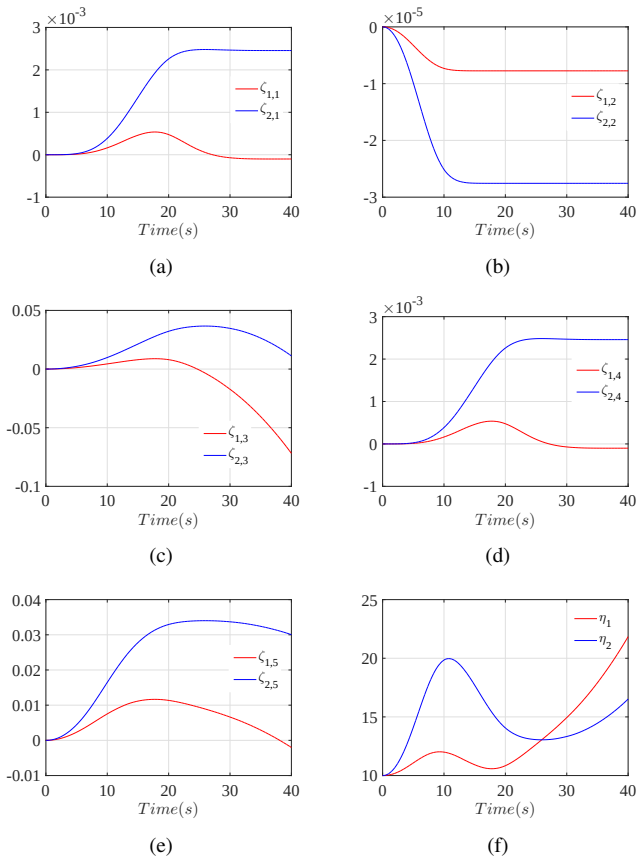


**FIGURE 6**. The decentralized scheme's parameter estimation for $\zeta_{i,w}$ and $\eta_i$ of both the upstream and downstream sets.

The values of $n_i$ used in the coupled centralized control inputs (Eq. 17) are listed in Table 1 and $\Gamma_i = \text{diag}[10]_{17\times17}$. The values of $\varepsilon_i$ utilized in developing the decentralized control inputs (Eq. 31) are given in Table 1 and selected to mitigate the effects of strong nonlinear interconnections among the sets which is inevitably a fundamental requirement of the decentralized scheme. For the centralized method, Figs. 4 and 5 present the estimation process of the unknown parameters ($\Theta_1$–$\Theta_{29}$) for both the upstream and downstream sets subject to the Initial$_1$ revealing the parameters convergence within the nominal operation time of 40(s); the Initial$_1$ yielded the coupled chaotic dynamics. The $\Theta_1$–$\Theta_{12}$ and $\Theta_{18}$–$\Theta_{29}$ indicate the sample parameters of the upstream and downstream sets, respectively. Note that the initial values of the parameters used in the centralized adaptation laws are 90% of their nominal values. Such initial values

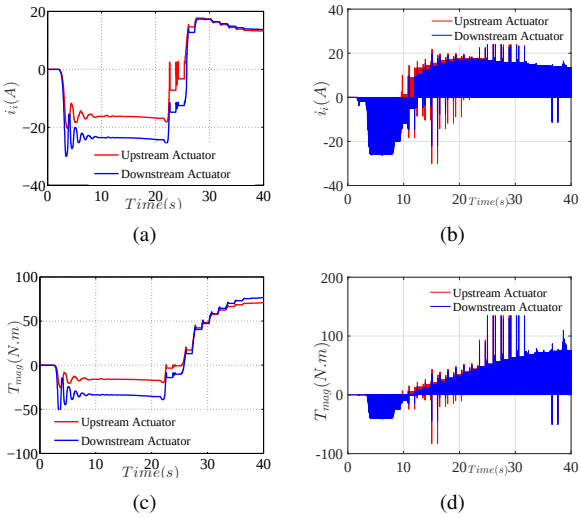


**FIGURE 7**. (a) The centralized control inputs; (b) The decentralized control inputs; (c) The centralized magnetic torques; (d) The decentralized magnetic torques.

are intentionally selected to yield meaningful estimated parameters with respect to the electro-magneto-mechanical-fluid nature of the network. It is of a great interest to observe that, despite the dominant chaotic dynamics resulted from the Initial$_1$, the parameters timely convergence and therefore, we expect to observe stable operations of both the coupled actuated valves. Note that both the centralized and decentralized approaches, based on the "sufficient richness" condition [31], would not exactly estimate the unknown parameters such that the schemes expectedly yield values to allow the desired task to be carried out.

Figs. 6(a) to 6(f) present the decentralized scheme's estimation process for $\zeta_{i,w}$ and $\eta_i$ of both the upstream and downstream sets. Note that some researchers have reported inefficiency [35] and lack of robustness of the decentralized schemes in the presence of strong nonlinear interconnections which are expected to be observed for the network subject to the chaotic/hyperchaotic dynamics. The estimated parameters validate the lack of robustness of the decentralized scheme in comparison with the centralized one. Few abrupt converging process of the parameters would potentially magnify the shortcomings of the decentralized scheme due to the significant effects of strong nonlinear interconnections between two sets. We hence expect to observe undesirable control inputs.

For the centralized scheme, the estimated parameters, based on Eq. 17, would help generate powerful control inputs, the applied currents of the bi-directional solenoid actuators ($i_i$), to vanish the chaotic dynamics of the interconnected sets (Fig. 2(a)) and then drive the coupled valves to track the desirable trajectories, which we addressed earlier (Eq. 7). Shown in Fig. 7(a) are the control inputs for both the upstream and downstream

actuators. As expected, the currents consist of two phases as shown in Fig. 7(a). The first phase, with oscillatory negative values of the currents, suppresses the coupled chaotic dynamics due to the Initial$_1$ resulting in downward/slightly upward motions of the plungers, which would consequently avoid the sudden jumps of the valves. During the second phase of the control process, the currents gradually take positive values indicating that the plungers move upward and therefore, the valves rotate toward the desirable trajectories. It is of a great interest to observe that the control input of the downstream set is remarkably higher than that of the upstream one, in particular for the first phase of the control process. The physical interpretation of such higher values of the control input used in the downstream set can be explained through the effects of the flow loads acting on the valve, in particular the hydrodynamic torque:

$$\frac{T_{h2}}{T_{h1}} \propto \left(\frac{D_{v2}}{D_{v1}}\right)^3 \times \left(\frac{c_{v1}}{c_{v2}}\right)^2 \tag{41}$$

$$\frac{T_{b2}}{T_{b1}} \propto \left(\frac{D_{v2}c_{v1}}{D_{v1}c_{v2}}\right)^2 \tag{42}$$

where $c_{v1}$ and $c_{v2}$ are the upstream and downstream valves' coefficients, respectively ($c_{vi}(\alpha_i) = p_i\alpha_i^3 + q_i\alpha_i^2 + o_i\alpha_i + \gamma_i$). We have previously reported [1–3, 9, 10, 12] that a smaller pipe diameter yields both the higher hydrodynamic and bearing torques due to the higher coefficient of the upstream valve than that of the downstream one (Eqs. 41 and 42). From another aspect, the hydrodynamic torque is a helping load [1–6, 8–13] to close the symmetric valve whereas the bearing one is a resistance (friction-based) torque for the valve's operation. The downstream set with a smaller pipe diameter, subject to the chaotic dynamics of the Initial$_1$, undoubtedly needs more suppressing control input to mitigate the destabilizer effects of the higher hydrodynamic torque acting on the valve. For the second phase of the control process, the higher resistance bearing torque acting on the downstream set inevitably demands slightly higher control input to push the valve to the desirable trajectory.

Such profiles of the control inputs of the centralized method for both the sets are expected to be observed for the driving magnetic torques (forces) as nonlinear functions of the control inputs in addition to the valves' rotation angles/plungers' displacements. Fig. 7(c) presents the centralized driving magnetic torques of both the coupled sets in which the two phases of the control process can be distinguished as we discussed for the currents. The oscillatory negative values of the magnetic torques suppress the chaotic dynamics along with mitigating the effects of the hydrodynamic torques. The positive magnetic torques (forces) move the plungers upward and subsequently, the valves move toward the desirable trajectories. The higher amount of the driving magnetic torque of the downstream set, for the second phase of the control process, looks logical to overcome the higher resistance bearing torque than that of the upstream one.

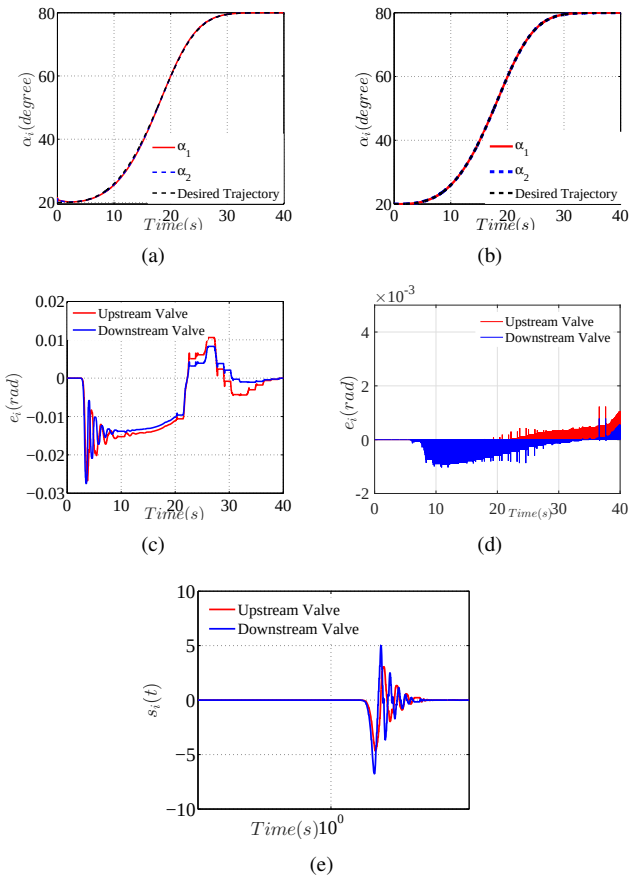


**FIGURE 8**. (a) The centralized valves' rotation angles; (b) The decentralized valves' rotation angles; (c) The centralized error signals; (d) The decentralized error signals; (e) The centralized combined tracking error signals.

Despite the centralized control inputs/magnetic torques, the decentralized scheme leads to the so-called "Bang-Bang" control inputs and magnetic torques shown in Figs. 7(b) and 7(d), respectively. Obviously, the implementation of the Bang-Bang control inputs for the network subject to the chaotic dynamics can be questionable and hence would probably not be feasible. As expected, such control inputs can result in failures of the actuation units and gradually damage the whole network. Note that the decentralized scheme yields slightly higher values of the Bang-Bang control inputs and magnetic torques than those of the centralized ones.

Shown in Fig. 8(a) are the upstream and downstream valves' rotation angles subject to the centralized scheme indicating that both the sets track the desirable trajectories (Eq. 7) by applying the control inputs which expectedly vanish the coupled chaotic dynamics due to the Initial$_1$. Both the error ($e_i$) and combined

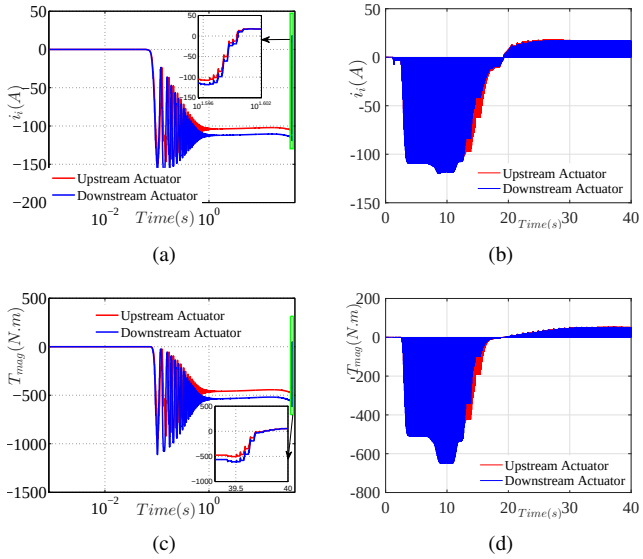


**FIGURE 9**. (a) The centralized control inputs; (b) The decentralized control inputs; (c) The centralized magnetic torques; (d) The decentralized magnetic torques.

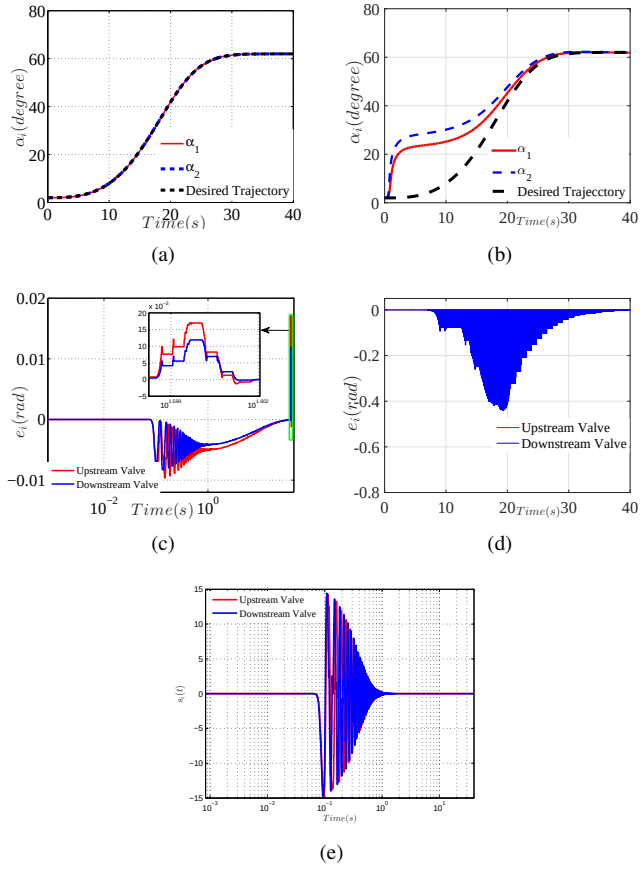


**FIGURE 10**. (a) The centralized valves' rotation angles; (b) The decentralized valves' rotation angles; (c) The centralized error signals; (d) The decentralized error signals; (e) The centralized combined tracking error signals.

tracking error ($s_i$) signals shown in Figs. 8(c) and 8(e), respectively, converge to zero revealing that the valves' angles ($\alpha_i$) tend to the desirable trajectories ($\alpha_{di}$) within the nominal operation time.

It is of a great interest to observe that the decentralized approach also pushes the valves to track the desirable trajectories (Figs. 8(b) and 8(d)) with even considerably smaller tracking errors. The tracking errors of the decentralized method are significantly smaller than those of the centralized one. Consequently, we deal with an important trade-off between the smaller tracking errors and Bang-Bang control inputs of the decentralized method in the presence of strong nonlinear interconnections and chaotic dynamics. This trade-off can be expected to become more crucial by adding more coupled sets. Another trade-off is computational cost of the centralized and decentralized schemes. Note that the computational time of the decentralized method, for only two sets, is almost one-sixtieth of the centralized one. It is straightforward to conclude that the computational cost of the decentralized scheme would be significantly lower than that of the centralized one by adding more interconnected sets subject to the chaotic dynamics. Therefore, the centralized adaptive method, by yielding smoother/practically feasible control inputs/magnetic torques and better robustness, is an effective approach in comparison with the decentralized one (even with smaller tracking error and computation time) to control the network of actuated butterfly valves subject to the chaotic dynamics.

Figs. 9(a) and 9(c) present the centralized control inputs and driving magnetic torques, respectively, used in vanishing the coupled hyperchaotic dynamics caused by the Initial$_2$ (Fig. 2(b)). As expected, the hyperchaotic dynamics of both the sets with the larger domains of attractions, which we have thoroughly addressed in [1,3], would require significantly higher values of the control inputs to be vanished than those of the chaotic ones.

The considerable control inputs expectedly result in the higher driving magnetic torques than the ones used in the network subject to the chaotic dynamics (Fig. 9(c)). The two phases of the control process, which we discussed for the chaotic case, can be observed for the hyperchaotic one such that the oscillatory negative control inputs/driving magnetic torques suppress the hyperchaotic dynamics. Note that the green boxes shown in Figs. 9(a) and 9(c) reveal the incremental values of the control inputs/torques to rotate the valves to the desirable trajectories.

The Bang-Bang control inputs/magnetic torques, which we discussed for the chaotic response, are expected to be observed for the network subject to the hyperchaotic dynamics. Shown in Figs. 9(b) and 9(d) expectedly reveal higher Bang-Bang con-

trol inputs/magnetic torques for the hyperchaotic responses than those of the chaotic ones; again due to the larger domains of attractions of both the sets.

Shown in Fig. 10(a) are both the upstream and downstream valves' rotation angles revealing that the valves' motions tend to the desirable trajectories (Eq. 8) subject to the centralized controller. Figs. 10(c) and 10(e) present the convergence of both the error and combined tracking error signals to zero, respectively. Consequently, it is straightforward to conclude that the centralized adaptation and control laws guarantee both the global stability of the coupled network and convergence of the tracking errors in which we analytically discussed in Section 3. Figs. 10(b) and 10(d) reveal that both the valves, by utilizing the decentralized controller, experience considerably higher tracking errors and, again for the hyperchaotic responses, the implementation of Bang-Bang control inputs can be potentially harmful.

## 5 Conclusions and Future Work

In this effort, we presented the novel sixth-order interconnected dynamic equations of the two coupled bi-directional solenoid actuated butterfly valves. The network underwent the harmful chaotic and hyperchaotic dynamics subject to some initial conditions and critical parameters of the equivalent viscous damping and the friction coefficient of bearing area. We then thoroughly studied both the centralized and decentralized adaptive schemes for different aspects of robustness, computational cost, and practically feasible control inputs. The issues of robustness and practical feasibility of control efforts expectedly become more critical in the presence of strong nonlinear interconnections among sets and harmful dynamical responses.

It was shown that the decentralized adaptive scheme yields significantly smaller tracking errors in comparison with the centralized one (for the chaotic dynamics) although the latter shows a much better performance by revealing more robust estimation process and feasible control inputs. The decentralized scheme, in the presence of chaotic/hyperchaotic dynamics, has the shortcomings of abrupt estimation process and, more importantly, Bang-Bang control inputs which would expectedly result in the failures of the coupled actuation units and gradually the whole network. Another trade-off is the computation cost of both the schemes. The computation time of the decentralized scheme, for this particular problem subject to the chaotic/hyperchaotic dynamics, is at least one-sixtieth of the centralized one and we expect to spend much lower computation time by adding more coupled agents. In summary, the decentralized controller needs to be utilized carefully, in particular for the systems subject to the interconnected chaotic and hyperchaotic dynamics.

We currently focus on developing the interconnected model of a network of $n$ actuated valves operating in series.

## REFERENCES


[1] Naseradinmousavi, P., Segala, D. B., and Nataraj, C., 2016. "Chaotic and hyperchaotic dynamics of smart valves system subject to a sudden contraction". *ASME Journal of Computational and Nonlinear Dynamics,* **11**(5), September, pp. 051025–051025–9.

[2] Naseradinmousavi, P., Krstic, M., and Nataraj, C., 2016. "Design optimization of dynamically coupled actuated butterfly valves subject to a sudden contraction". *ASME Journal of Mechanical Design,* **138**(4), April, pp. 041402–041402–11.

[3] Naseradinmousavi, P., Machiani, S. G., Ayoubi, M. A., and Nataraj, C., 2017. "Coupled operational optimization of smart valve system subject to different approach angles of a pipe contraction". *Journal of Structural and Multidisciplinary Optimization,* **55**(3), pp. 1001–1015.

[4] Naseradinmousavi, P., 2015. "A novel nonlinear modeling and dynamic analysis of solenoid actuated butterfly valves coupled in series". *ASME Journal of Dynamic Systems, Measurement, and Control,* **137**(1), January, pp. 014505–014505–5.

[5] Naseradinmousavi, P., and Nataraj, C., 2013. "Optimal design of solenoid actuators driving butterfly valves". *ASME Journal of Mechanical Design,* **135**(9), July, pp. 094501–094501–5.

[6] Naseradinmousavi, P., and Nataraj, C., 2012. "Transient chaos and crisis phenomena in butterfly valves driven by solenoid actuators". *Journal of Communications in Nonlinear Science and Numerical Simulation,* **17**(11), November, pp. 4336–4345.

[7] Lee, D., Naseradinmousavi, P., and Nataraj, C., 2012. "Nonlinear model-based adaptive control of a solenoid-valve system". *Journal of Control Science and Engineering,* **2012**.

[8] Naseradinmousavi, P., and Nataraj, C., 2011. "Nonlinear mathematical modeling of butterfly valves driven by solenoid actuators". *Journal of Applied Mathematical Modelling,* **35**(5), pp. 2324–2335.

[9] Naseradinmousavi, P., Krstic, M., Bagheri, M., and Nataraj, C., 2016. "Coupled chaotic and hyperchaotic dynamics of actuated butterfly valves operating in series". In The ASME 2016 Dynamic Systems and Control Conference, Vol. 2, p. V002T17A001.

[10] Naseradinmousavi, P., Bagheri, M., and Nataraj, C., 2016. "Coupled operational optimization of smart valve system subject to different approach angles of a pipe contraction". In The ASME 2016 Dynamic Systems and Control Conference, Vol. 1, p. V001T02A001.

[11] Naseradinmousavi, P., and Nataraj, C., 2015. "Design optimization of solenoid actuated butterfly valves dynamically coupled in series". In Proceedings of the ASME 2015 Dynamic Systems and Control Conference, Vol. 2, p. V002T33A001.

[12] Naseradinmousavi, P., 2015. "Optimal design of solenoid actuated butterfly valves dynamically coupled in series". In Proceedings of the ASME 2015 International Mechanical Engineering Congress & Exposition, Vol. 4A: Dynamics, Vibration, and Control, p. V04AT04A032.

[13] Naseradinmousavi, P., and Nataraj, C., 2011. "A chaotic blue sky catastrophe of butterfly valves driven by solenoid actuators". In Proceedings of the ASME 2011 International Mechanical Engineering Congress & Exposition, Vol. 7: Dynamic Systems and Control; Mechatronics and Intelligent Machines, Parts A and B, pp. 25–31.

[14] Chen, Y. H., 1992. "Decentralized robust control for large-scale uncertain systems: A design based on the bound of uncertainty". *ASME Journal of Dynamic Systems, Measurement, and Control,* **114**(1), March, pp. 1–9.

[15] Ramiirez, G. G., and Tang, Y., 2002. "Decentralized control of rigid robots driven by current-fed induction motors". *ASME Journal of Dynamic Systems, Measurement, and Control,* **124**(4), December, pp. 549–553.

[16] Chen, Y. H., 1991. "Decentralized adaptive robust control design: The uncertainty is time varying". *ASME Journal of Dynamic Systems, Measurement, and Control,* **113**(3), September, pp. 515–518.

[17] Yan, J.-J., 2003. "Memoryless adaptive decentralized sliding mode control for uncertain large-scale systems with time-varying delays". *ASME Journal of Dynamic Systems, Measurement, and Control,* **125**(2), June, pp. 172–176.

[18] Hua, C., Guan, X., and Shi, P., 2005. "Robust decentralized adaptive control for interconnected systems with time delays". *ASME Journal of Dynamic Systems, Measurement, and Control,* **127**(4), March, pp. 656–662.

[19] Karpenko, M., Sepehri, N., and Anderson, J., 2007. "Decentralized coordinated motion control of two hydraulic actuators handling a common object". *ASME Journal of Dynamic Systems, Measurement, and Control,* **129**(5), January, pp. 729–741.

[20] Elmahdi, A., Taha, A. F., Sun, D., and Panchal, J. H., 2015. "Decentralized control framework and stability analysis for networked control systems". *ASME Journal of Dynamic Systems, Measurement, and Control,* **137**(5), May, pp. 051006–1–051006–11.

[21] Ghasemi, A. H., Hoagg, J. B., and Seigler, T. M., 2016. "Decentralized vibration and shape control of structures with colocated sensors and actuators". *ASME Journal of D,* **138**(3), January, pp. 031011–1–031011–11.

[22] Hernandez, R., Salas, O. S., and DeLeon, J., 2017. "Decentralized formation control based on adaptive super twisting". *ASME Journal of Dynamic Systems, Measurement, and Control*.

[23] Ioannou, P. A., 1986. "Decentralized adaptive control of interconnected systems". *IEEE Trans. Autom. Control,* **AC-31**(4), April, pp. 291–298.

[24] Fu, L. C., 1993. "Robust adaptive decentralized control of robot manipulators". *IEEE Trans. Autom. Control,* **57**(3), January, pp. 106–110.

[25] Wang, B., Shi, K., Zhang, C., and Zhu, D., 2015. "Fuzzy generalized predictive control for nonlinear brushless direct current motor". *ASME Journal of Computational and Nonlinear Dynamics,* **11**(4), pp. 041004– 041004–7.

[26] Luo, R., and Zeng, Y., 2015. "The control and synchronization of a class of chaotic systems with output variable and external disturbance". *ASME Journal of Computational and Nonlinear Dynamics,* **11**(5), pp. 051011–051011–7.

[27] Reddy, B. S., and Ghosal, A., 2015. "Asymptotic stability and chaotic motions in trajectory following feedback controlled robots". *ASME Journal of Computational and Nonlinear Dynamics,* **11**(5), pp. 051012–051012–11.

[28] Khamsuwan, P., and Kuntanapreeda, S., 2016. "A linear matrix inequality approach to output feedback control of fractional-order unified chaotic systems with one control input". *ASME Journal of Computational and Nonlinear Dynamics,* **11**(5), pp. 051021–051021–7.

[29] Naseradinmousavi, P., 2012. "Nonlinear modeling, dynamic analysis, and optimal design and operation of electromechanical valve systems". PhD thesis, Villanova University, May.

[30] Nayfeh, A. H., and Balachandran, B., 1995. *Applied nonlinear dynamics: analytical, computational, and experimental methods*. Wiley-VCH Verlag GmbH, Germany.

[31] Slotine, and Li, 1991. *Applied Nonlinear Control*. Prentice-Hall.

[32] Karimi, B., Menhaj, M. B., Karmi-Ghartemani, M., and Saboori, I., 2009. "Decentralized adaptie control of large-scale affine and nonaffine nonlinear systems". *IEEE Transactions on Instrumentation and Measurement,* **58**(8), August, pp. 2459–2467.

[33] Spooner, J. T., and Passino, K. M., 1996. "Adaptive cnotrol of a class of decentralized nonlinear systems". *IEEE Transactions on Automatic Control,* **41**(2), February, pp. 280–284.

[34] Karimi, B., Menhaj, M. B., Karmi-Ghartemani, M., and Saboori, I., 2007. "A decentralized direct adaptive conntroller for a class of large-scale interconnected nonlinear systems". In Proc. IEEE Int. Symp. Intell. Signal Process, pp. 265–270.

[35] Tarau, A. N., Schutter, B. D., and Hellendoorn, J., 2009. "Centralized, decentralized, and distributed model predictive control for route choice in automated baggage handling systems". *Control Engineering and Applied Informatics (Special Issue on Distributed Control in Networked Systems),* **11**(3), pp. 24–31.